Advances in Radiation Oncology (2025) **10**, 101793

advances in radiation oncology

www.advancesradonc.org

Scientific Article

Monitoring of Early Skin Reactions by Optical Coherence Tomography and Dermatoscopy in Patients Receiving Radiation Therapy for Head and Neck Cancer

Bettina Heise, PhD,[a,b,*] Peter Schlagnitweit, MSc,[a] Robert Pollak, DI,[a] Karoline Felbermayer, DI,[b] Elisabeth Silberberger, Mag,[c] Lukas Kocik, MD,[c] Leonhard Trinkl, BSc,[c] David Weinzinger, DI,[c] Philipp Anderlik, DI,[c] Andreas Springer, PhD,[c] Marija Geroldinger-Simic, MD, PhD,[d,e] Georg Gruber, MD, PhD,[c] Maximilan Hartl, MD,[f] and Hans Geinitz, MD[c,e]

[a]Institute for Mathematical Methods in Medicine and Data Based Modelling, Johannes Kepler University (JKU), Linz, Austria; [b]Research Center for Non-Destructive Testing (RECENDT)-GmbH, Linz, Austria; [c]Department of Radiation Oncology, Ordensklinikum Linz (OKL), Barmherzige Schwestern, Linz, Austria; [d]Department of Dermatology, Ordensklinikum Linz (OKL), Elisabethinen, Linz, Austria; [e]Medical Faculty, Johannes Kepler University (JKU), Linz, Austria; and [f]Department of ENT, Ordensklinikum Linz (OKL), Barmherzige Schwestern, Linz, Austria

Received 11 July 2024; accepted 11 April 2025

Purpose: Patients with head and neck cancer undergoing radiation therapy (RT) may experience pronounced acute skin reactions. We tested whether optical coherence tomography (OCT) and dermatoscopy could detect and monitor early subclinical RT-induced skin changes and might be used as a noninvasive prediction tool for higher-grade acute toxicity.

Methods and Materials: Handheld OCT and dermatoscopy were used to monitor skin conditions during RT in head and neck cancer patients. Images were reviewed for typical and suspicious features facilitated by electronic image analyses. Radiation toxicity was graded weekly by a radiation oncologist. Machine learning was used to analyze the recorded data and to extract features, patterns/anomalies, and risk prediction values for high-grade radiation toxicity.

Results: The most common skin features during RT observed by OCT were expressions of hyperkeratosis, blister formation, and in selected cases, formation of extensive microvascular structures or stratification disorder. Dermatoscopy revealed an almost linear increase in skin redness and saturation over the course of RT. By integrating all imaging and clinical data from RT weeks 1 to 3, it was possible to predict an increased risk of severe radiation toxicity (National Cancer Institute Common Terminology Criteria for Adverse Events (CTCAE) grade 3 or higher) in the second half of RT. A prediction accuracy of 72%, 75%, and 77% was achieved with OCT and clinical assessment, dermatoscopy and clinical assessment, and all 3 modes combined, respectively.

Sources of support: We thank the Oberösterreichischen Krebshilfe; the Fachgruppe Onkologie der Vinzenz Gruppe; and the Fahl GmbH for financial support of this study. Additionally, this project is financed by research subsidies granted by the government of Upper Austria (FTI 2022 HIQUAMP: Wi-2021-303205/13-Au). Supported by Johannes Kepler Open Access Publishing Fund.

Research data are stored in an institutional repository and will be shared upon request to the corresponding author.

*Corresponding author: Bettina Heise, PhD; Email: Bettina.Heise@jku.at

https://doi.org/10.1016/j.adro.2025.101793

Conclusions: OCT and dermatoscopy can detect early radiation-induced skin changes at a subclinical level. Dermatoscopy is more accessible, whereas OCT requires training and further electronic processing to interpret images. Dermatoscopy, but not OCT, can quantify skin color changes, whereas OCT is able to deliver unique information on epidermal suspicious microstructural changes.

Introduction

Radiation therapy (RT) equipment and planning schemes are becoming increasingly more sophisticated, but skin toxicity still occurs,[1] especially in areas, such as the neck or chest. In patients with an individual higher sensitivity to (radiograph) radiation or a genetic predisposition,[2] more severe inflammatory skin reactions and higher levels of radiation toxicity have been described.[3] Severely affected patients would require additional health care measures to reduce or manage acute adverse effects during RT.

Clinically detectable skin reactions caused by ionizing radiation that can be observed in the acute inflammatory phase include erythema, dry and moist desquamation, loss of hair follicles, and in some cases ulceration,[4,5] as well as effects on the dermal-epidermal junction.[6]

In order to monitor acute skin reactions and altered skin conditions associated with RT, imaging methods such as dermatoscopy and optical coherence tomography (OCT) are viable options. OCT, which is a noninvasive imaging technique, operates with near-infrared light.[7] In the last decades, OCT has been established as a valuable tool for dermatologic diagnosis,[8,9] partly replacing biopsies[10] and enabling the visualization of diverse inflammatory and cancerous skin diseases.[11,12] OCT imaging for acute radiation dermatitis detection has been briefly presented.[13] A preclinical study performed in irradiated in vitro skin models was published,[14] comparing capabilities of OCT and histologic sectioning techniques.

Machine learning (ML) methods have become increasingly prevalent in the field of RT to facilitate and accelerate RT planning and data analysis.[15,16]

Our study compared OCT and dermatoscopic imaging in their capabilities for monitoring early acute skin reactions in head and neck cancer (HNC) patients receiving definitive or postoperative RT.

Methods and Materials

Participants

Patients with HNC treated with definitive or postoperative RT or radio-chemotherapy were eligible. Patients with malignant tumors in the pharynx, larynx, or oral cavity treated with definitive or postoperative RT or radio-chemotherapy between June 2020 and June 2022 were suitable for the study (see Table 1). The main exclusion criteria were: concomitant application of radiation sensitivity-enhancing agents (C225 cetuximab), apparent skin disease, severe redness of the skin or an exulcerated tumor in the measurement region, strong beard growth, pronounced scar formation, pigmentation or a tattoo in the measurement region.

All patients provided written informed consent to participate in the study. The study was cleared by the local ethics committee (EKS39/18) and registered on ClinicalTrials.gov ID: NCT04610645. Of 229 HNC patients treated at our department within the recruiting period, 60 eligible patients were addressed to take part in the study. The main reason for not addressing patients was organizational reasons (longer periods of recruiting stops because of the COVID-19 pandemic and OCT machine dysfunction). Of the 60 addressed patients 33 agreed to take part in the study and 3 of those retracted before measurements and treatment started. Most patients declined because of the additional time requirements of about 30 minutes per measurement. This rather low rate of participation has to be seen in the light of the COVID-19 pandemic.

All participants were Caucasians with Fitzpatrick skin scale types 1 to 3.

Sample size and study aim

For this explanatory study, the target size was set to 30 participants. The aim of the study was to visualize and quantify subclinical changes within the dermis and epidermis in irradiated HNC patients using OCT. A further purpose was to create prediction models for higher-grade acute toxicity from imaging and clinical data collected during the first weeks of RT.

Treatment

Target volumes were contoured according to Grégoire et al.[17] Additionally, PTVs were cropped at 2 mm within the body surface. Planning was carried out with the Varian Eclipse planning system (version 15.6) using the Acuros dose calculation algorithm (15.6.05). All patients received volumetric intensity modulated RT with 6 to 10 MeV photons from a linear accelerator. Most patients received simultaneous integrated boost treatment. For concomitant RChT, cisplatin 40 mg/m^2 was given weekly.

The applied radiation dose was measured for the first patient in vivo with a set of metal−oxide−semiconductor

Table 1 Panel of HNC patients monitored in the clinical study

Participants: 30 head and neck tumor patients	
Age	**47-80 y (mean: 61.5 y.)**
Sex	9 females, 21 males
HNC entity	Oropharyngeal: 18 patients Hypopharyngeal: 2 patients Parotid gland: 1 patient Palate: 1 patient Oral cavity: 4 patients Larynx-carcinoma: 3 patients CUP: 1 patient
Radio-(chemo-)therapy treatment regime	With chemotherapy: 19 patients Without chemotherapy: 11 patients
Extent of elective nodal clinical target volume	Unilateral: 13 patients Bilateral: 14 patients No elective nodal irradiation/RT of (laryngeal) primary tumor only: 3 patients
Fractionation	R(Ch)T definitive or after R2-resection (15 patients): SIB with 70 Gy at primary site and gross nodes, 63 Gy at intermediate risk areas (positive lymph node levels); 56 Gy at nodal regions at risk of microscopic spread in 35 fractions (Fx). Laryngeal cancer (3 patients): 65.25 Gy in 29 Fx (no elective lymph nodes) (1 patient) With parotid cancer SIB for 30 Fx at 2 Gy and sequential boost on primary site with 3 × 2 Gy (1 patient) With high radiation sensitivity: 29 Fx SIB (single dose reduced from 2 Gy to 1.8 Gy in high dose area and 1.6 Gy ~~if~~ cervical after RTd13; 54.8 Gy in high dose area and 49 Gy ~~if~~ cervical) Postoperative R(Ch)T R0/R1-resection (10 patients): SIB 60 Gy at primary site and intermediate risk areas (positive lymph node levels), 54 Gy at nodal regions at risk of microscopic spread in 30 Fx
Skin type (Fitzpatrick scale)	Grade 1: 1 patient Grade 2: 28 patients Grade 3: 1 patient

Abbreviations: HNC = head and neck cancer; RT = radiation therapy; SIB = simultaneous integrated boost.

field-effect transistor (MOSFET) detectors (left and on the right side of the neck). Dose measurements were carried out at the same place where the OCT probe was placed. This was assured by a circular punching in the immobilization mask through which the probe as well as the MOSFET was positioned. Additionally, we used a dose build-up cap, to obtain the dose in 1.5 cm in depth, reducing uncertainties caused by dose surface effects. The difference between the measured and the calculated dose was about 10% on the skin surface and it was 6% for a depth of 1.5 cm. Based on our experience with in vivo dosimetry using MOSFET detectors, we judge the differences between measurements and calculation as sufficiently accurate.

Treatment characteristics including skin/surface dose are given in Appendix E1, Table E1.

Imaging

OCT

A handheld OCT (Lumedica, OQ Labscope 2.0) operating at a central wavelength of 800 nm was used for monitoring purposes. The wavelength range was selected as a compromise between a higher resolution at the cost of a lower imaging depth. The OCT device has a moderate scan rate of 10 B-scans per second and is capable of performing volume imaging, as well as time series and averaging. Its lateral imaging field is 7 × 5 mm, with a lateral resolution of 18 μm and an axial resolution of 8 μm in air. The OCT imaging technique enables the monitoring of structural features and alterations in the dermis and epidermis. It records gray-scale cross-sectional scans at a depth of approximately 1 to 2 mm into the skin. From these cross-sectional images, radiomic features, including local mean intensities, statistical values, and textural features, can be extracted.

A patch-wise 3 × 3 imaging scheme was employed for OCT imaging, with the procedure being carried out on the left and right neck skin regions, see Fig. 1a. The use of a patterned mask ensured a high degree of stability in registration, which remained consistent over the course of the RT time frame. In the case of dermatoscopy, a patch-wise 2 × 2 scheme imaging approach was selected, with the images being coregistered to the scanned OCT

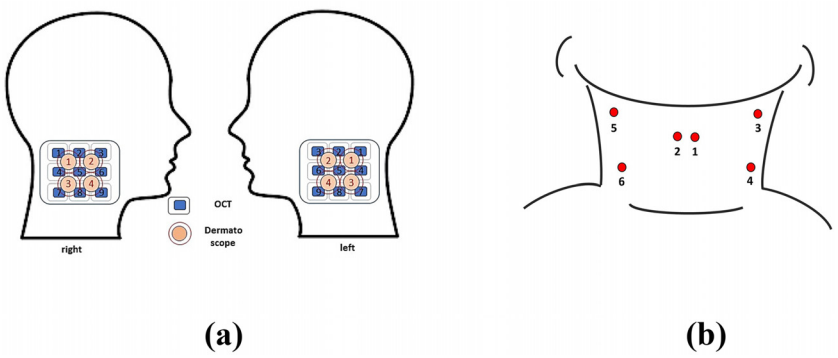

Figure 1 The scanning scheme for optical coherence tomography (OCT) and dermatoscopic imaging: (a) the scan scheme as a 3 × 3 and 2 × 2 configuration, respectively, typically recorded on head and neck cancer radiation therapy patients; in contrast, (b) the scanning scheme for laryngeal carcinoma radiation therapy patients as a left/middle/right neck-side scheme.

regions. In the case of patients who received diagnoses of laryngeal carcinoma, an imaging scheme comprising 2 positions—right/center and left/center—was employed, see Fig. 1b. For each imaging session, the schemes provide 9 OCT volume sets and 4 dermatoscopic skin images for each side of the neck, and 6 OCT volume sets and 6 dermatoscopic skin images for laryngeal carcinoma patients, respectively. The initial participant was initially scanned with a slightly different positioning scheme; however, this proved to be impractical and was therefore replaced by the 3 × 3 patch-wise scanning method.

Dermatoscopy

A commercially available dermatoscope (Heine iC1) was used for skin imaging, capturing color images in the conventional Red Green Blue (RGB) color space at a skin surface area of approximately 10 × 10 mm^2. The dermatoscopic RGB images were subsequently transferred to the Hue Saturation Value (HSV) color space, employing the standard RGB to HSV color space conversion.[18] The mean and variance of the hue, saturation, and intensity values of each HSV image were calculated using an in-house program code. The HSV representation was found to be more suitable than the RGB representation in this context. For further details, see Appendix E2.

Scanning frequency

Initial image scanning for the first 10 patients was conducted on each RT day. A subsequent interim analysis was conducted in order to find the optimal scanning frequency per week. The goal was to find a good compromise between workload for the staff and patient occupancy on the one hand and predictive performance on the other hand. Performance was evaluated by simulating different scanning frequencies based on the already acquired data. We found that a reduction in scanning frequency from 5 to only 3 times per RT week best suited the needs of all stakeholders, without many tradeoffs in performance.

Toxicity assessment

Patients were evaluated on a weekly basis to record adverse treatment effects. Toxicity was graded according to the National Cancer Institute Common Terminology Criteria for Adverse Events, version 5[19] criteria by a radiation oncologist with expertise in HNC therapy. In order to establish a correlation with imaging data, the maximum toxicity score for either dermatitis or mucositis grade was applied.

Data analysis and ML

For mathematical image analysis and model generation, a total of 450 data sets were aggregated. Each data set typically consisted of 9 volume OCT image stacks, which were acquired in accordance with the specified scanning scheme, as illustrated in Fig. 1. In addition to the volume images, 9 time-averaged cross-sectional OCT images and 4 dermatoscopy images, recorded each on both sides of the neck, were analyzed. The image data were incorporated into the analysis, along with the clinical assessment data (CTA-AE score).

The OCT image data underwent a preprocessing phase with the objective of reducing the potential impact of imaging artifacts, including those associated with autocorrelation and oversaturation, see also Appendix E2, Fig. E1. Approximately 10% of the OCT data were rejected or lost because of stronger imaging errors, a defective device, incomplete data sets, or other reasons. Consequently, 7082 OCT volume sets recorded at different time points were ultimately available for analysis and learning.

The radiomic features for OCT images were extracted on a patch-by-patch basis using the open-source software Py-Feat.[20] The features for dermatoscopy images were

determined with an in-house Matlab script. For further details, see Appendix E2, Table E2.

In the context of ML for data analysis, 3 classical ML methods were employed: (1) random forest (RF),[21] (2) extreme gradient boosting (XGB),[22] and (3) deep learning through convolution neural networks (CNN).[23] These methods were also reported for model generation in the context of OCT-supported bioimaging.[24-26]

The ML models were generated during our study for 2 distinct use scenarios:

- To identify patients with rare morphologic and structural skin features (ie, outlier or anomaly detection within an RT treatment group) by applying all 3 models (XGB, RF, CNN) based on the data gathered up to the second RT week.
- To predict, based on the data gathered up to the third RT week, the risk of experiencing high-grade RT acute toxicity (ie, dermatitis or mucositis grade 3 or more). Here, the XGB model was applied.

Further details on the data handling and ML specifications can be found in Appendix E2 (Table E3, Fig. E2).

Results

Findings from dermatoscopic imaging

The majority of patients exhibited grade 2 maximum skin toxicity and grade 2 maximum mucositis. For details, see Appendix E3, Table E4. The observed development of toxicity is consistent with previously published data.[27,28]

The progression of acute radiation dermatitis and mucositis over the course of RT is illustrated for 3 cases with varying degrees of toxicity, as depicted in Fig. 2a. The dermatoscopic image sequence, recorded over a period of 5 weeks for a single patient exhibiting grade 4 skin toxicity, is presented in Fig. 2b. The relationship between saturation and radiation toxicity was confirmed through the analysis of the HSV data. The correlation between the mean saturation and the acute skin radiation toxicity grade was determined for all participants and quantified as $\rho_{corr} = 0.52$, with a P value $P<.01$. It is noteworthy that the correlation between mean saturation and the grade of radiation dermatitis was more pronounced than the correlation between mean hue and the grade of radiation dermatitis ($\rho_{corr} = 0.15$, $P < .01$), as determined across all participants. This is further evidenced by the box-plot statistics presented in Fig. 2c. The correlation matrix between all considered features is provided in Appendix E2, Fig. E3.

Findings from OCT imaging

The qualitative OCT findings for the studied HNC-RT patients were similar to the findings reported by histologic biopsies.[29,30]

RT therapy induced hyperkeratosis, which became evident from RT week 3 to 4 onward, expressed in OCT B-scans as strongly grainy and bright microstructures at the highly reflective stratum corneum, whereas at the RT start, the stratum corneum was manifested as a bright, continuous surface line (see Fig. 3a).

The formation of blisters and vesicles was a notable finding, visible on OCT in RT weeks 4 to 6 for the majority of the patients. However, in some cases, particularly in patients with high-grade radiation toxicity, this blister formation was already evident from RT week 3 onward (see Fig. 3b).

The visibility of dermal-epidermal junction in OCT images has been found to be significantly influenced by the scattering behavior of the epidermal and dermal layers. Variations in visibility have been observed between patients, potentially because of differences in their individual skin status in the neck region and as a consequence of RT. In some cases, an epidermal layer disorder or epidermal thickening was noted during the second half of the RT period (see Fig. 3c).

For skin exhibiting moderate scattering behavior, microvascular patterns within the dermal papillary layer were discernible as dark structures (among a predominantly white/scattering dermal layer) in OCT cross-sectional images (see Fig. 4). In a smaller patient cohort (n = 3), a more pronounced manifestation of microvascular patterns and edema-like structures was discerned during RT (see Fig. 4a). These characteristics, which were initially subtle at the onset of RT but became increasingly evident as the treatment progressed. Follicular structure alterations during the RT period,[31] were observed in some participants, though not in all (see Fig. 4b).

A concise overview of the visual findings is presented in Table 2. Further illustrations are provided in Appendix E3, Figs. E5-E9.

Detection of outliers/anomalies

Based on the recorded image and toxicity assessment data for a selected group under consideration (comprising 8 participants with a similar treatment scheme), the 3 models provided comparable information content, as illustrated in Fig. 5a. Two patients in the considered group were identified by each ML method with a high probability (ie, greater than 80%) as outliers, or as exhibiting a deviation from the "average" group pattern. However, the ML-based finding for such anomalies was not specific for high-grade radiation dermatitis, but also for an increasing

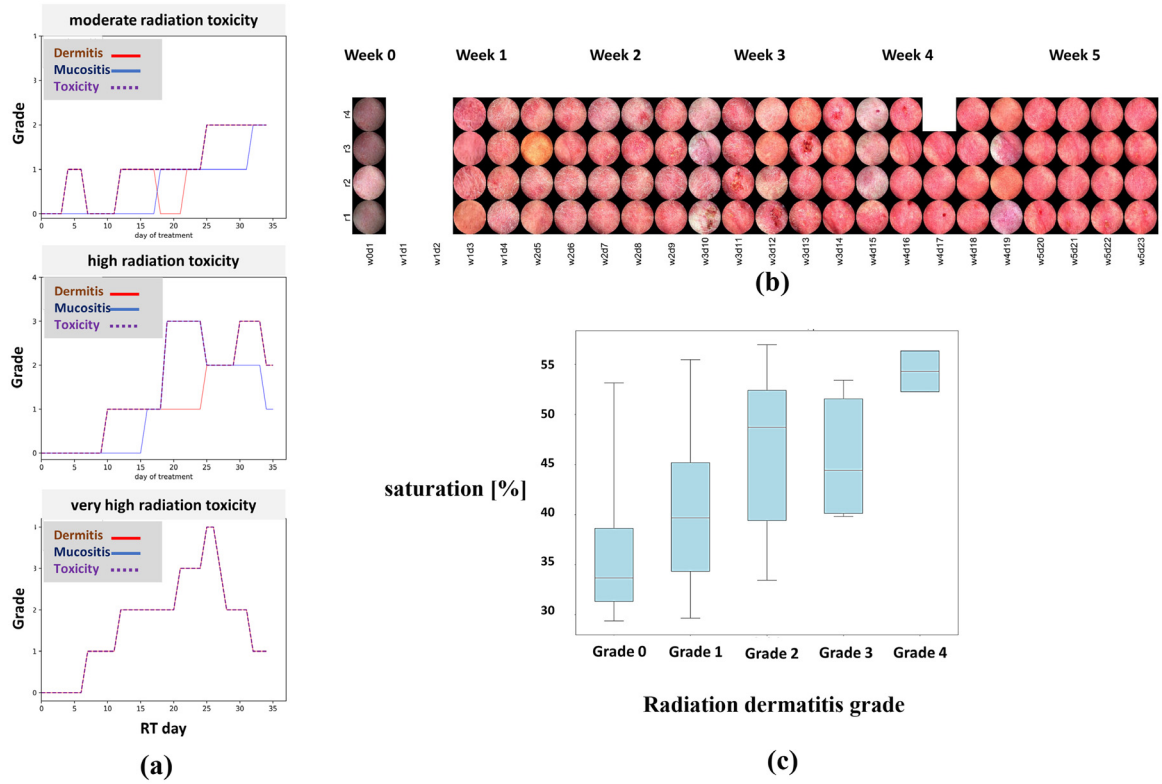

Figure 2 Courses of National Cancer Institute Common Terminology Criteria for Adverse Events classified grades of: (a) radiation dermatitis, radiation mucositis and maximum radiation toxicity (derived from the maximum of both dermatitis and mucositis grade), based on a weekly expert assessment and spanning the radiation therapy (RT) period: demonstrating 3 typical severity courses: (top) moderate, (middle) high, (bottom plot) very high severity course of radiation toxicity (in the case of the patient exhibiting a particularly high level of severity, only the radiation dermatitis was assessed on a weekly basis); (b) a series of dermatoscopic images, captured between the first and fifth weeks of RT treatment and exemplified for the patient exhibited a markedly elevated level of skin toxicity, ie, radiation dermatitis grade 4, throughout the course of RT; (c) correlation between mean saturation and radiation dermatitis as classified by the National Cancer Institute Common Terminology Criteria for Adverse Events scale over the course of RT (with IQR box; whiskers: maximum/minimum, line: median), calculated for all 30 participants together, resulting in a Pearson correlation value $\rho_P = 0.52$ and a P value $P < .01$. Considering individually the 30 participants, one participant showed a negative correlation, and one participant showed a P value greater than .01.

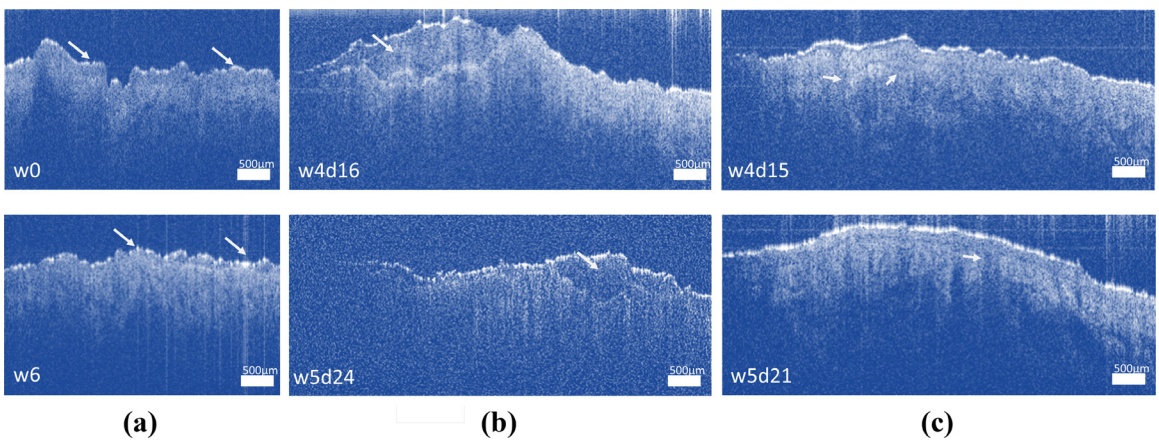

Figure 3 Optical coherence tomography B-scans exemplifying: (a) unaffected skin with a normal, rather smooth stratum corneum at radiation therapy (RT) beginning (week 0 (w0)) (top scan); affected skin with bright grainy patterned stratum corneum and a hyperkeratotic finding at RT week 6 (w6) (bottom scan); (b) blister formation for a patient at the site of high skin radiation toxicity at RT week 4 (w4) (top scan) and RT week 5 (w5) (bottom scan); (c) epidermal layer disordering with a wavy (top scan) and straight (bottom scan) manifestation of dermal-epidermal junction (DEJ); (see the white arrowheads respectively).

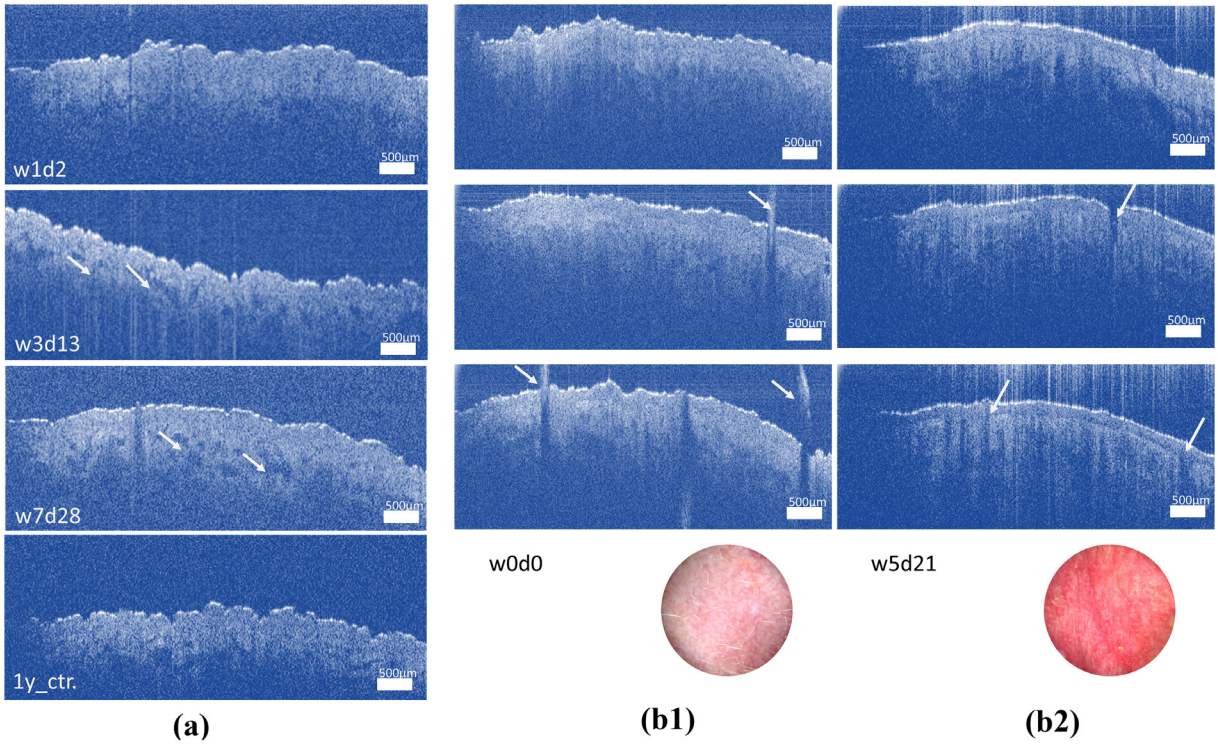

Figure 4 Optical coherence tomography B-scans exemplifying quantitative findings: (a) a broadening of (blood/lymphatic) microvessel structures during radiation therapy (RT) period and (recovered) normal status at control after 1 year, (top-down scans: RT week 1 (w1), week 3 (w3), week 7 (w7), and control (ctr.) 1 year); (b) changes in hair follicular structures and frequency (top-down: recorded at different scanning positions) for (b1) RT week 0 (w0) (white arrows pointing to hairs and hair shafts), and (b2) RT week 5 (w5) (white arrows pointing to "empty" underlying follicular structures), and the corresponding dermatoscopic images.

appearance of microvessel structures, as illustrated in Fig. 5b.

The RF and XGB models exhibited the highest accuracy for anomaly detection, with 76.6% ± 11.6% and 76.6% ± 11.9%, respectively. The convolutional neural network (CNN) model exhibited the lowest accuracy, with 72.9% ± 9.5%. This outcome also reflects the restricted quantity of training data, which exerts a lesser influence on both classical ML tools (RF and XGB) in comparison to the CNN method, which typically necessitates a substantial amount of data for training.

The XGB model was selected as the optimal model for predicting the risk of high-grade radiation toxicity

Table 2 Prominent findings from OCT and dermatoscopy

Finding	Number of patients with finding
OCT imaging (total 29 patients)	
(Hyper)keratosis/dandruff/grainy structures	8 (27.6%)
Pronounced epidermal thickening/keratinization	2 (6.9%)
Blister and vesicles	7 (24.1%)
Vessel size/appearance increase	3 (10.3%)
Stratum corn. detached or epidermal layer disorder	8 (27.6%)
Dermatoscopy (total 29 patients)	
Very high-redness/saturation	5 (17.2%)
Stronger crusting/wed desquamations	3 (10.3%)

Abbreviations: OCT = optical coherence tomography.
The appearance before RT was used for visual comparison. Several findings can be detected in the same patient. Of the total of 30 participants, one patient had no dermatoscopy recordings and one had no OCT recordings; therefore, 29 patients were included.

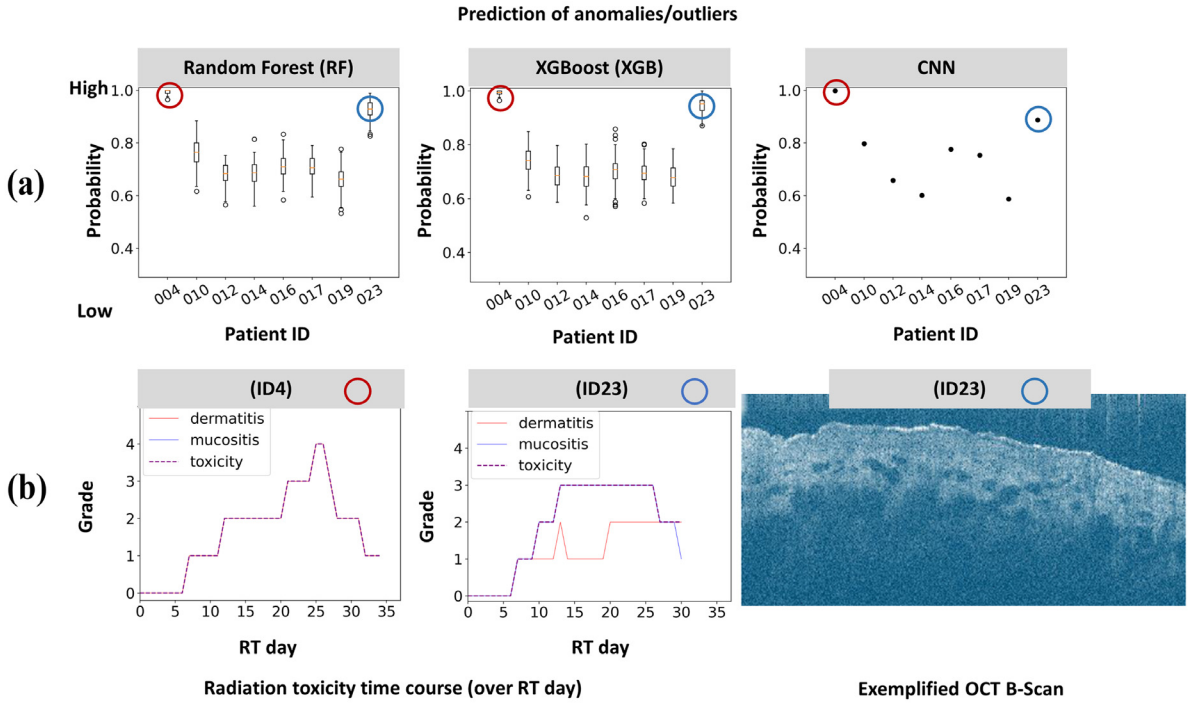

Figure 5 Anomaly detection: (a) detection results/probabilities for possible anomalies, obtained by the random forest (RF), extreme gradient boosting (XGB), and convolution neural network (CNN) models, within a radiation therapy (RT) treatment group (consisting of 8 members here). Patients with potential anomalies are similarly found by each model, ie, highest probability values (red/blue circle labeled). (b) Verifying the 2 highest probability cases (with probability >80%), which point out the following: (1) a patient reaching the following extremely high grade of skin toxicity (grade 4) in the second half of RT (red circle labeled); (2) a patient with moderate/high grade of skin toxicity, but disclosing suspicious and over RT enhanced (microvessel) structural patterns, visible in optical coherence tomography (OCT) cross-sectional image (blue circle labeled). For patient ID4, only the radiation dermatitis was assessed weekly.

(radiation dermatitis and mucositis, respectively) because of its superior computational efficiency and robust performance even with limited data.

Prediction of risk of increased acute radiation toxicity by ML

The XGB model was employed to predict grade 3 or higher maximum radiation toxicity (maximum of acute skin or mucosa toxicity) based on imaging and toxicity data derived during the first 3 treatment weeks. To validate the prediction model, the accuracy, the area under the curve, the sensitivity, and the specificity were selected as performance metrics, derived from the receiver operating characteristic curves[32] and confusion/error matrices.

The influence of varying frequencies of image data acquisitions on the performance metric values is presented in Table 3. The influence of varying combinations/aggregations of image data is presented in Table 3. The respective values in terms of the prediction accuracy of grade 3+ acute toxicity yield: 72% (OCT and medical expert data), 75% (dermatoscopy and medical expert data), and 77% (dermatoscopy and OCT and medical expert data).

For further details as well as for the receiver operating characteristic graphical plots and the error matrix, see Appendix E2, Fig. E4.

Discussion

The objective of the study was: (1) to assess the feasibility of OCT to visualize and quantify subclinical and microscopic changes in the epidermis and dermis during clinical RT, and (2) to analyze whether early changes in skin structure and color as detected by OCT and dermatoscopy might be used in conjunction with clinical assessment to predict grade 3+ acute toxicity later in the course of treatment. OCT provides a means of monitoring cutaneous structural changes at a microscopic level. Structural alterations of the skin (summarized in Table 2), including blister formation, desquamation, and epidermal layer disorders were observed as expressions of acute inflammatory skin reactions during the second half of the RT

Table 3 Prediction performance metric for varying frequency of image data acquisition and combination of data types, respectively

Frequency of data acquisitions (for OCT and dermatoscopy and clinical toxicity assessment data combined)		
4 times in the first 10 RT days	**6 times in the first 15 RT days**	**10 times in the first 15 RT days**
ACC: 0.75	ACC: 0.77	ACC: 0.85
AUC: 0.80	AUC: 0.83	AUC: 0.90
Sensitivity: 0.72	Sensitivity: 0.74	Sensitivity: 0.88
Specificity: 0.79	Specificity: 0.80	Specificity: 0.79
Combination of data types (for an image acquisition frequency of 6 times in the first 15 RT days)		
Radiation toxicity assessment data only	OCT data only	Dermatoscopy data only
ACC: 0.59	ACC: 0.69	ACC: 0.72
AUC: 0.60	AUC: 0.73	AUC: 0.80
Sensitivity: 0.50	Sensitivity: 0.79	Sensitivity: 0.80*
Specificity: 0.69	Specificity: 0.58	Specificity: 0.64
Balanced: 0.595	Balanced: 0.685	Balanced: 0.72
OCT and radiation toxicity assessment data combined	Dermatoscopy and radiation toxicity assessment data combined	OCT, dermatoscopy, and radiation toxicity assessment data combined
ACC: 0.72	ACC: 0.75	ACC: 0.77*
AUC: 0.78	AUC: 0.83	AUC: 0.83*
Sensitivity: 0.75	Sensitivity: 0.79	Sensitivity: 0.74
Specificity: 0.68	Specificity: 0.71	Specificity: 0.80*
Balanced: 0.715	Balanced: 0.75	Balanced: 0.77*

Abbreviations: ACC = accuracy; AUC = area under the curve; OCT = optical coherence tomography; RT = radiation therapy.
*Higherst performance value

period (mainly weeks 5-6). A subset of patients showed the emergence of high-grade radiation dermatitis, with these inflammatory changes manifesting as early as the third RT week. In the literature, alterations in skin scattering features have also been documented.[33] Alterations in scattering coefficients were qualitatively assessed but not quantitatively validated in this study.

Dermatoscopic imaging offered insights into the changing characteristics of skin color, indicating a linear increase in the saturation value during RT. Moreover, a strong correlation was observed between saturation and early clinical skin toxicity. As all participants included in this study had Fitzpatrick type 1 to 3 skin color, it remains unclear, whether this association would also be seen in individuals with type 4 or higher skin pigmentation. With regard to OCT, skin pigmentation seems to have little influence on structural visibility and imaging depth.

In order to predict the risk of high-grade acute skin toxicity, it should be noted that the combination of dermatoscopy and clinical radiation toxicity assessment exhibited superior performance in comparison to OCT and toxicity assessment. However, the incorporation of all 3 recorded data types (i.e., OCT, dermatoscopy, and clinical assessment) yielded optimal results in terms of the quality parameters, including accuracy, the area under the curve, and specificity. The sensitivity, however, is less in the combined model as compared to dermatoscopy and clinical evaluation alone. As saturation is a prominent feature of the performance of dermatoscopy, its benefit might be different for persons with skin types other than those included in the study.

The added value of OCT is also based on its ability to provide epidermal and subepidermal structural information on suspicious skin microformations without the need for biopsies. This might facilitate "continuous" skin observation on a microscopic level—for example, in studies using novel technologies and products to reduce radiation toxicity or eventually in clinical routine.

Weaknesses of the study

It is acknowledged that the cohort of 30 HNC patients under observation is of limited size. We deliberately included only patients with HNC in the study as they are most likely to develop higher-grade acute radiation skin toxicity. By protocol, the sample size was limited to 30 patients as this was an explanatory study and our main aim was to

establish the feasibility of OCT in detecting microscopic structural skin changes during RT similar to those previously described in histologic examinations using invasive biopsy devices. In addition, we analyzed whether early morphologic and skin color changes might be predictive for later occurring (acute) toxicity, knowing that this was merely a proof of principle in a very limited, artificial setting. Neither comorbidity/comedication nor any specific treatment or dose characteristics were entered into the model. One might argue that these factors potentially affect early morphologic/color changes and maximum acute toxicity in the same way, but this has to be proven in further studies. Also, the sample size did not allow us to generate a large amount of interindividual image data in order to train and validate ML models more extensively.

The OCT image data exhibited considerable variability in their characteristics between the participants in this study. This variability may be attributed to the differences in age, health status, and general skin condition among the patients, as well as to the involvement of different staff for OCT recording. Consequently, the results must be interpreted with caution to prevent overgeneralization.

Conclusions

In conclusion, our study demonstrated the feasibility of OCT and dermatoscopy in monitoring radiation-induced skin changes at a subclinical level during the treatment course. The approach can offer early insights into radiation effects that may, in the future, assist medical experts in applying supportive measures or adapted RT planning. Further automation of OCT imaging and verification of its prognostic value in larger patient cohorts might pave the way toward a broader clinical application.

Disclosures

The authors declare that they have no known competing financial interests or personal relationships that could have appeared to influence the work reported in this paper.

Acknowledgments

We want to acknowledge Rainer Leitgeb/MU Vienna for helpful discussions at the beginning of this study and Astrid Hochholdt for the initial work in image preprocessing. Peter Schlagnitweit was responsible for statistical analysis.

Supplementary materials

Supplementary material associated with this article can be found in the online version at doi:10.1016/j.adro.2025.101793.

References

1. Bray FN, Simmons BJ, Wolfson AH, Nouri K. Acute and chronic cutaneous reactions to ionizing radiation therapy. *Dermatol Ther (Heidelb)*. 2016;6:185-206.
2. Rzepka D, Schenker H, Geinitz H, et al. Chromosomal radiosensitivity in oncological and non-oncological patients with rheumatoid arthritis and connective tissue diseases. *Radiat Oncol*. 2023;18:98.
3. Brook I. Early side effects of radiation treatment for head and neck cancer. *Cancer Radiother*. 2021;25:507-513.
4. Chan RJ, Webster J, Chung B, Marquart L, Ahmed M, Garantziotis S. Prevention and treatment of acute radiation-induced skin reactions: A systematic review and meta-analysis of randomized controlled trials. *BMC Cancer*. 2014;14:53.
5. Hymes SR, Strom EA, Fife C. Radiation dermatitis: Clinical presentation, pathophysiology, and treatment 2006. *J Am Acad Dermatol*. 2006;54:28-46.
6. Oguchi M, Komura J, Ofuji S. Ultrastructural studies of epidermis in acute radiation dermatitis. Basal lamina thickening and coated vesicles. *Arch Dermatol Res*. 1978;262:73-81.
7. Fercher AF. Optical coherence tomography. *J Biomed Opt*. 1996;1:157-173.
8. Ziolkowska M, Philipp CM, Liebscher J, Berlien HP. OCT of healthy skin, actinic skin and NMSC lesions. *Med Laser Appl*. 2009;24:256-264.
9. Mogensen M, Thrane L, Jørgensen TM, Andersen PE, Jemec GBE. OCT imaging of skin cancer and other dermatological diseases. *J Biophotonics*. 2009;2:442-451.
10. Brezinski ME, Tearney GJ, Bouma BE, et al. Optical coherence tomography for optical biopsy. Properties and demonstration of vascular pathology. *Circulation*. 1996;93:1206-1213.
11. Psomadakis CE, Marghoob N, Bleicher B, Markowitz O. Optical coherence tomography. *Clin Dermatol*. 2021;39:624-634.
12. Olsen J, Holmes J, Jemec GBE. Advances in optical coherence tomography in dermatology—A review. *J Biomed Opt*. 2018;23:1-10.
13. Photiou C, Strouthos I, Cloconi C. Early detection of acute radiation dermatitis (ARD) using in vivo optical coherence tomography (OCT) images. *Biophotonics Congress: Biomedical Optics 2022 (Translational, Microscopy, OCT, OTS, BRAIN)*. Technical Digest Series, Optica Publishing Group; 2022.
14. Bromberger L, Heise B, Felbermayer K, et al. Radiation-induced alterations in multi-layered, in-vitro skin models detected by optical coherence tomography and histological methods. *PLoS One*. 2023;18:e0281662.
15. Fiandra C, Cattani F, Leonardi MC, et al. Machine learning for predicting clinician evaluation of treatment plans for left-sided whole breast radiation therapy. *Adv Radiat Oncol*. 2023;8:101228.
16. Schwartz D, Sawyer TW, Thurston N, Barton J, Ditzler G. Ovarian cancer detection using optical coherence tomography and convolutional neural networks. *Neural Comput Appl*. 2022;34:8977-8987.
17. Grégoire V, Ang K, Budach W, et al. Delineation of the neck node levels for head and neck tumors: A 2013 update. DAHANCA, EORTC, HKNPCSG, NCIC CTG, NCRI, RTOG, TROG consensus guidelines. *Radiother Oncol*. 2014;110:172-181.
18. Dubois E. Various color spaces, representations, and transformations. In: Dubois E, ed. *The Structure and Properties of Color Spaces and the Representation of Color Images*. Springer; 2010:61-71.
19. U.S. Department of Health and human Services. Common Terminology Criteria for Adverse Events v5.0 (CTCAE). 2017. Accessed XXX. https://ctep.cancer.gov/protocoldevelopment/electronic_applications/docs/ctcae_v5_quick_reference_5x7.pdf.
20. Py-Feat. Py-Feat: Python Facial Expression Analysis Toolbox. Accessed January 16, 2025. https://py-feat.org/pages/intro.html.
21. Breiman L. Random forests. *Mach Learn*. 2001;45:5-32.
22. Chen T, Guestrin C. XGBoost: A. *scalable tree boosting system*KDD '16: Proceedings of the 22nd ACM SIGKDD International Conference on Knowledge Discovery and Data Mining. Association for Computing Machinery; 2016:785-794.

23. Yu H, Yang LT, Zhang Q, Armstrong D, Deen MJ. Convolutional neural networks for medical image analysis: State-of-the-art, comparisons, improvement and perspectives. *Neurocomputing*. 2021;444:92-110.
24. Bayhaqi YA, Hamidi A, Canbaz F, Navarini AA, Cattin PC, Zam A. Deep learning models comparison for tissue classification using optical coherence tomography images: Toward smart laser osteotomy. *OSA Continuum*. 2021;4:2510-2526.
25. Liu X, Ouellette S, Jamgochian M, Liu Y, Rao B. One-class machine learning classification of skin tissue based on manually scanned optical coherence tomography imaging. *Sci Rep*. 2023;13:867.
26. Majumdar A, Allam N, Zabel WJ, Demidov V, Flueraru C, Vitkin IA. Binary dose level classification of tumour microvascular response to radiotherapy using artificial intelligence analysis of optical coherence tomography images. *Sci Rep*. 2022;12:13995.
27. Carr CM, Benson JC, DeLone DR, et al. Manifestations of radiation toxicity in the head, neck, and spine: An image-based review. *Neuroradiol J*. 2022;35:427-436.
28. Lee N, Chuang C, Quivey JM, et al. Skin toxicity due to intensity-modulated radiotherapy for head-and-neck carcinoma. *Int J Radiat Oncol Biol Phys*. 2002;53:630-637.
29. Olascoaga A, Vilar-Compte D, Poitevin-Chacón A, Contreras-Ruiz J. Wound healing in radiated skin: Pathophysiology and treatment options. *Int Wound J*. 2008;5:246-257.
30. Borrelli MR, Shen AH, Lee GK, Momeni A, Longaker MT, Wan DC. Radiation-induced skin fibrosis: Pathogenesis, current treatment options, and emerging therapeutics. *Ann Plast Surg*. 2019;83:S59-S64.
31. Lin SJ, Yue Z, Paus R. Clinical pathobiology of radiotherapy-induced alopecia: A guide toward more effective prevention and hair follicle repair. *J Invest Dermatol*. 2023;143:1646-1656.
32. Hajian-Tilaki K. Receiver operating characteristic (ROC) curve analysis for medical diagnostic test evaluation. *Caspian J Intern Med*. 2013;4:627-635.
33. Guo X, Bu P, Wang X, et al. Scattering imaging of skin in Fourier domain optical coherence tomography. *Opt Commun*. 2013;305:137-142.